Electronic Supplementary Information (ESI)†

Experimental Evidence of Charged Domain Walls in Lead-free Ferroelectric Ceramics: Light-driven Nanodomain Switching

Fernando Rubio-Marcos[†,*], Adolfo Del Campo[†], Rocío E. Rojas-Hernandez[†, ∥], Mariola O. Ramírez[§], Rodrigo Parra[‡], Rodrigo U. Ichikawa[#], Leandro A. Ramajo[‡], Luisa E. Bausá[§] and Jose F. Fernández[†].

[†] *Electroceramic Department, Instituto de Cerámica y Vidrio, CSIC, Kelsen 5, 28049 Madrid, Spain*

[∥] *Departamento de Engenharia Química/CQE, Instituto Superior Tecnico/UL, Lisboa, Portugal*

[§] *Department of Física de Materiales and Instituto Nicolás Cabrera, Universidad Autónoma de Madrid, 28049 Madrid, Spain*

[‡] *Instituto de Investigaciones en Ciencia y Tecnología de Materiales (INTEMA), Av. Juan B Justo 4302 (B7608FDQ), Mar del Plata, Argentina*

[#] *Instituto de Pesquisas Energ éticas e Nucleares, IPEN-CNEN/SP, Butantã, São Paulo, SP, 05508-000, Brazil*

*Correspondence and requests for materials should be addressed to F. R-M (email: frmarcos@icv.csic.es

Supplementary Figures

S1 Synchrotron radiation X-ray diffraction (SR-XRD)

High-resolution synchrotron X-ray diffraction data was taken at XRD1 beamline at LNLS Light Source in Campinas, Brazil. The range was from 1.208° up to 121.180°, with 0.004 steps using photon energy of 12 keV at room temperature. The refined wavelength using NIST LaB_6 standard reference material was of 1.033200(1) Å. Rietveld refinement was performed using the General Structure Analysis System (GSAS) program with the EXPGUI graphical user interface,[1,2] in order to obtain the full width-at half-maximum (FWHM) of the diffraction peaks. For the profile fitting, the modified Tompson–Cox–Hastings pseudo-Voigt (TCH-pV) [3] function was used. The (Θ) independent Gaussian term (GW), and (cosΘ) and (tanΘ)- dependent Lorentzian terms (Lx and LY, respectively) were refined.[4] Unit cell parameters, scale-factors, background and coefficients corresponding displacement and zero-shift correction were also refined. The background was fitted with a linear interpolation function with 9 coefficients.

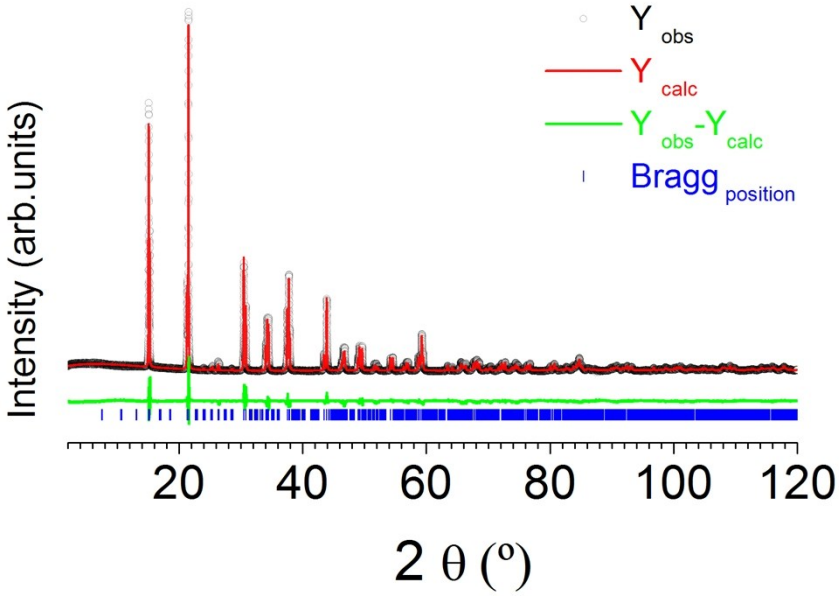

Figure S1 | Crystallographic characterization of KNN Ferroelectric Ceramic by High-resolution synchrotron X-ray diffraction. Experimental (circles), calculated (continuous red line), and difference (continuous green line at bottom of each panel) neutron diffraction patterns of KNN ceramic collected at Room Temperature, the incident wavelength is 1.033200Å, and the positions of Bragg peaks are indicated by vertical blue bars.

Synchrotron X-ray diffraction confirmed the crystal structure of the KNN ceramic to be monoclinic (M_C) with a $K_{0.1}Na_{0.9}NbO_3$ chemical composition. For the refinement a single phase was tested using a M_C symmetry and a space group *P1m1*. The KNN (M_C) ceramic has a monoclinic *c/a* polydomain structure with average lattice parameters of a = 7.8608 Å, b= 7.7755 Å and *c* = 7.8533 Å (see **Table S1**). The existence of the polydomain structure is further confirmed using Confocal Raman Microcopy (CRM) as described in the main manuscript. We summarized in **Table S1** the structural parameters of KNN sample derived from the Rietveld analysis of high-angular resolution x-ray powder patterns. In **Figure S1** is shown prototypical example of the Rietveld refinement at room temperature of the $K_{0.1}Na_{0.9}NbO_3$ structure. The final refinements are satisfactory in which R_{wp}-factor, "R-weighted pattern", and GOF, "Goodness of fit indicator", (reliable factor based on the integrated intensity) are fairly reduced. In addition, visual results of the plots show the accomplishment of the Rietveld refinement, as reflected by small differences between calculated and observed (see **Fig. S1**). Note that even small Bragg reflections are quantitatively reproduced.

Table S1 | Lattice parameters and convergence *R factors* (Figures-of-merit) and GOF goodness-of-fit index obtained by diffractogram refined data of the KNN ceramic.

Sample	***a*** (Å)	***b*** (Å)	***c*** (Å)	**β** (º)	**γ** (º)	**α** (º)	$\mathbf{R_{wp}}$ (%)	**GOF**
$\mathbf{K_{0.1}Na_{0.9}NbO_3}$	7.8608(1)	7.7755(1)	7.8533(1)	90	90.5444(13)	90	12.37	3.47

S2 Domains in ceramics structures

The Field Emission Scanning Electron Microscopy image (FE-SEM, Hitachi S-4700), shown in **Figure S2a**, illustrates the microstructure of the KNN ceramic, which was sintered at 1125 °C for 2 h. From **Fig. S2a**, it can be observed that the ceramic has a dense microstructure and a typical feature of quadrate shaped grains, which are common in KNN-based ceramics. A grain size distribution, GSD, of the ceramic is shown in the **Fig S2b**. The ceramic shows a bimodal GSD indicating a coexistence of two kinds of grain population. So, GSD reveals that the average grain size is ~6.7 ± 3 μm. In addition, through a classical approach for polycrystalline sample (ceramic), we can establish that the domain width (*d*) can be roughly expressed by the correlation: $d \sim \sqrt{a}$ (that is, domain widths, *d*, scale as the square root of the grain size, *a*).[5-6] In view of the above correlation, for an average grain size of a ~ 6.7 μm (our case) the *d* calculated value should be ca. 2.5 μm, as shown in **Fig. S2c**.

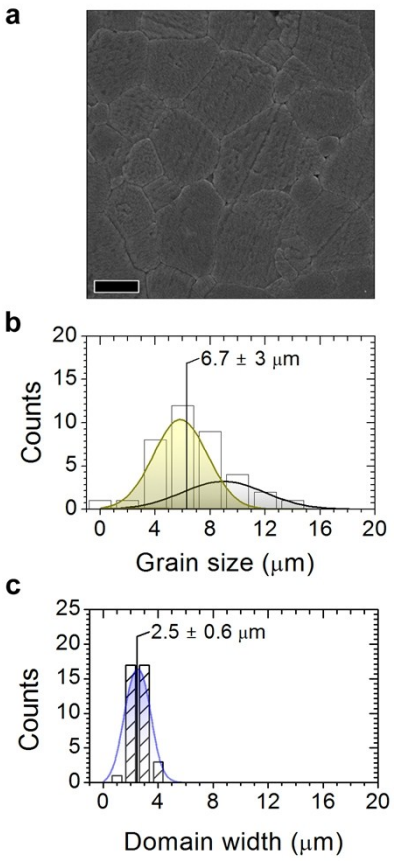

Figure S2 | Microstructural characterization of the KNN ceramic. a, Microstructure of polished and thermally etched surface of KNL-NTS sintered ceramic at 1125 ºC during 2 hours. As can be observed from panel S2a, the sample has a dense microstructure with cuboidal shaped grains, which is a common feature in KNL-NTS based ceramics. Scale bar, 4 μm. The panel **b** of the Fig. shows the grain size distribution (GSD) of KNN ceramic. The GSD is fitted to the sum of two Gaussian peaks because of the system presents a bimodal distribution. **c** Domain width distribution, *d*, of KNN ceramic calculated from the grain size measured by FE-SEM.

S3 Experimental observation of the anomaly generated by the appearance of charged domain walls

The strain gradient of the ferroelectric domain (**Figure S3a**) is a consequence of the combination of different effects. First effect, the appearance of alternate in-plane and out-of-plane regions produces alternation of the Raman shift value of the A_{1g} Raman mode. The in-plane ferroelectric domains are constricted and therefore the polarization is reduced. By the contrary, in the out-of-plane domains, the polarization increase as a consequence of the ability of the domain to growth. **Figure S3b** summarized schematically this alternation. Second effect, the presence of CDWs modifies the polarization in the way that strongly CDWs enhanced the polarization and therefore the blueshift of Raman signal meanwhile weakly CDWs reduced such a Raman signal (**Fig. S3c**). By a combination of both effects it is possible to simulate the evolution of the Raman shift of A_{1g} Raman mode across the ferroelectric domains (**Fig. S3d**). The simulated evolution explains the strain gradient response of the experimental evolution. Differenced between the simulated and the experimental evolution are attributed to the limited optical resolution of the CRM (typically 230 nm).

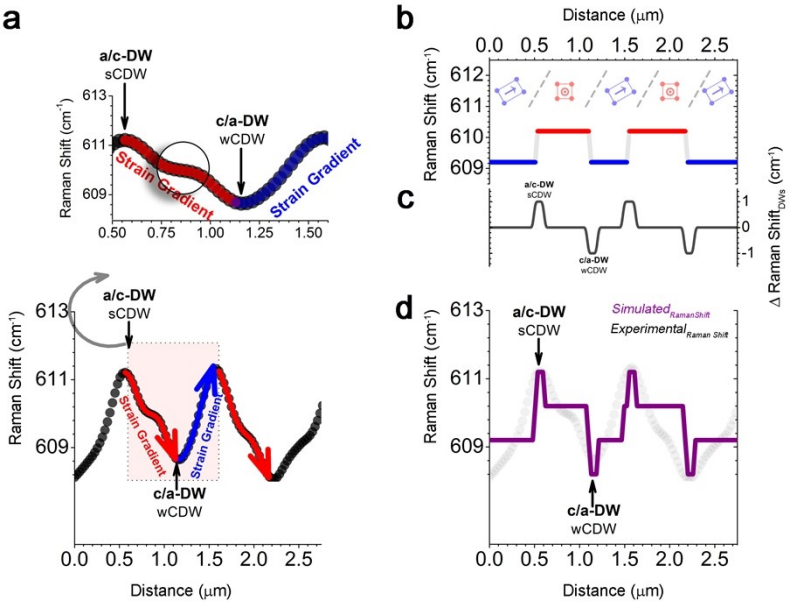

Figure S3 | Charged Domain Walls Contribution to the Polarization Gradient on the Domain Structure. a, Evolution of the Raman shift of the A_{1g} mode showing the existence of a strain gradient into the ferroelectric domains, which reaches a maximum at *a/c*-domain wall (its evolution is represented by a red arrow), and a minimum strain value at *c/a*-domain wall (its evolution is marked with a blue arrow). This line-scanned profile of the Raman shift evolution of each ferroelectric domain corresponding to the white dashed arrows of the Figs. 2a of the main manuscript. In the main panel is shown a strongly charged wall (sCDW), which is associated with a head-to-head 90º domain wall. Whereas the weakly charged domain walls (wCDW) has a tail-to-tail. Moreover, the insets in the top of panel a show the existence of an anomaly on strain gradient associated with the presence of a strongly charged wall (sCDW). **b**, represent schematically the contribution of the alternate in-plane and out-of plane domain regions to the Raman shift of the A_{1g} Raman mode. **c**, represent schematically the contribution of the alternate strongly and weakly CDWs to the Raman shift of the A_{1g} Raman mode and d represent schematically the resulting Raman shift evolution of the A_{1g} Raman mode across the ferroelectric domains as a result combination of the alternate in-plane and out-of plane domain regions plus the contribution CDWs in comparison with the experimental curve (signaled in grey).

S4 Ferroelectric domain switching in ceramic materials by applying an electrical field: A classical approach.

As described in the main manuscript, ferroelectric materials tend to develop domains in order to reduce stresses and depolarization field. Due to these domains, often the overall polarization is zero and no piezoelectric response can be measured. Therefore it is desirable to orient the domains to one general direction. This can be done by applying a sufficiently electrical field (above the coercive field, Ec) that would bring about switching of the polarization vector of each domain to the nearest permitted direction according to their symmetry (**see Figure S4**). In polycrystalline materials, where the crystallographic orientation of the grains is random with respect to one another, optimized poling conditions are of great importance. When external electrical field is applied, application (in z-direction), non-180ºdomain switching occurs and produces a net elongation (with respect to the before poling state) along z compatibly to the orientation of the domains. The domain orientation is determined by the underlying native grain orientation of the material, which influences domain switching, and thus produces a certain net elongation.[7-8]

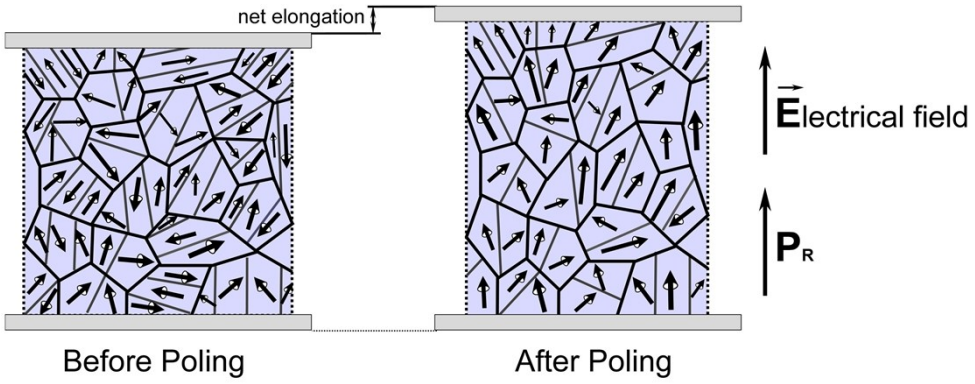

Figure S4 | Ferroelectric domain switching in ceramic materials by applying an electrical field. Schematic representation showing the effect of electrical field application on a polycrystalline ferroelectric with random orientated grains. Arrows indicate the directions of domain polarisations within each grain. In the pictures on the right (i.e. after E-field application), polarisation directions before and after E-field application are indicated with solid arrows. Upon electrical field application (in z-direction), non-180ºdomain switching occurs and produces a net elongation along z compatibly to the orientation of the domains at the remnant state.

Supplementary References

(1) Dreele, R. Von; Larson, A. *General Structure Analysis System (GSAS)*; 2004.

(2) Toby, B. H. EXPGUI, a Graphical User Interface for GSAS. *J. Appl. Crystallogr.* **34**, 210–213 (2001).

(3) Thompson, P.; Cox, D. E.; Hastings, J. B. Rietveld Refinement of Debye-Scherrer Synchrotron X-Ray Data from Al_2O_3. *J. Appl. Cryst.* **20**, 79–83 (1987).

(4) Young, R. A.; Wiles, D. B. Profile Shape Functions in Rietveld Refinements. *J.Appl. Cryst*. **15**, 430–438 (1982).

(5) Arlt, G. Twinning in ferroelectric and ferroelastic ceramics: stress relief. *J. Mater. Sci.* **25**, 2655-2666 (1990)

(6) Catalan, G., Seidel, J., Ramesh, R. & Scott, J. F. Domain wall nanoelectronics. *Rev. Mod. Phys.* **84**, 119-156 (2012).

(7) Damjanovic, D., Ferroelectric, dielectric and piezoelectric properties of ferroelectric thin films and ceramics. *Reports on Progress in Physics*. **61**, 1267-1324 (1998).

(8) Kaufmann, P., Röhrig, S., Supancic, P., Deluca, M. Influence of ferroelectric domain texture on the performance of multilayer piezoelectric actuators. *J. Eur. Ceram. Soc.* **37**, 2039-2046 (2017) 4125-4129.